Bioelectrochemistry 149 (2023) 108285

Contents lists available at ScienceDirect

Bioelectrochemistry

journal homepage: www.journals.elsevier.com/bioelectrochemistry

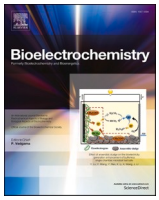

Elucidating the interaction of antidepressant drug paroxetine with ct-dsDNA: A comparative study by electrochemical, spectroscopic, and molecular docking approaches

Rafia Nimal [a,b], Didem Nur Unal [b,c], Cem Erkmen [b,c], Sevinc Kurbanoglu [b], Muhammad Siddiq [a], Gokcen Eren [d], Afzal Shah [a], Bengi Uslu [b,*]

[a] Quaid-i-Azam University, Department of Chemistry, Islamabad 45320, Pakistan
[b] Ankara University, Faculty of Pharmacy, Department of Analytical Chemistry, 06560 Ankara, Turkey
[c] Ankara University, The Graduate School of Health Sciences, Ankara 06110, Turkey
[d] Gazi University, Faculty of Pharmacy, Department of Pharmaceutical Chemistry, 06330 Ankara, Turkey

ARTICLE INFO

Keywords:
DNA Biosensor
Drug-DNA interaction
Fluorescence spectroscopy
Paroxetine
Voltammetry

ABSTRACT

This study is designed to investigate the interaction of phenylpiperidine derivative drug paroxetine, which is an effective serotonin reuptake inhibitor and biomolecules through electrochemical, fluorescence spectroscopy, and molecular docking methods. The interaction between paroxetine and biomolecules was investigated by differential pulse voltammetry according to the decrease in deoxyguanosine anodic oxidation signal of double-stranded calf thymus DNA. Fluorescence spectroscopy studies were performed by titrating paroxetine against double-stranded calf thymus DNA solution at four different temperatures. The fluorescent results showed that paroxetine had a great affinity to bind with double-stranded calf thymus DNA. Interaction studies demonstrate that paroxetine binds to double-stranded calf thymus DNA via intercalation binding mode, and the binding constant values were calculated as 7.24×10^4 M^{-1} and 1.52×10^4 M^{-1} at 25 °C, based on voltammetric and spectroscopic results, respectively. Moreover, with the aim of elucidating the interaction mechanism between paroxetine and double-stranded calf thymus DNA, electrochemical and fluorescence spectroscopy studies along with molecular docking analysis were made.

1. Introduction

The discovery of electrical activity in nucleic acids leads to the development of various electrochemical approaches for the analysis and quantification of nucleic acids [1]. In recent years nucleic acids have been largely employed as tools for recognizing and monitoring several compounds of analytical value. Layers of nucleic acid integrated over the electrochemical transducers can give rise to unique affinity biosensors for molecules of small molecular weight [2–5]. The action of these devices thus depends upon the interactions that took place between the surface-immobilized DNA and the target drugs and aid the rapid screening of these drugs [1].

One crucial aspect of pharmaceutical development processes and drug discovery is drug-DNA interaction [4]. The binding of DNA with small aromatic ligands can occur primarily through three interaction modes, including electrostatic interaction, intercalation, and groove binding [6]. The electrostatic interaction is largely non-specific and involves the negatively charged nucleic sugar-phosphate structure. The intercalation mode of interaction involves the intercalation of planar aromatic ring systems into the base pairs. This intercalation mode is commonly found in organic molecules with planar geometry and comprising of a number of aromatic condensed rings like daunomycin [7], doxorubicin [8], echinomycin [9], bleomycin [10], etc. Groove binding is found among the drugs that interact with minor and major grooves of DNA double helix. ± Minor groove binding results in strong connectivity with the groove walls and strong electrostatic interactions like mithramycin, netropsin [11], etc., while ± Major groove binding as observed in the case of norfloxacin bring about hydrogen bonding to the DNA, establishing a DNA triple helix. The nature and strength of the interaction largely affect the therapeutic action of the targeted nucleic acid. Electrochemical response of DNA prior to the addition of drugs and after the interaction can thus be used for the evaluation of the

* Corresponding author.
E-mail address: buslu@pharmacy.ankara.edu.tr (B. Uslu).

https://doi.org/10.1016/j.bioelechem.2022.108285
Received 3 January 2022; Received in revised form 28 September 2022; Accepted 2 October 2022
Available online 10 October 2022

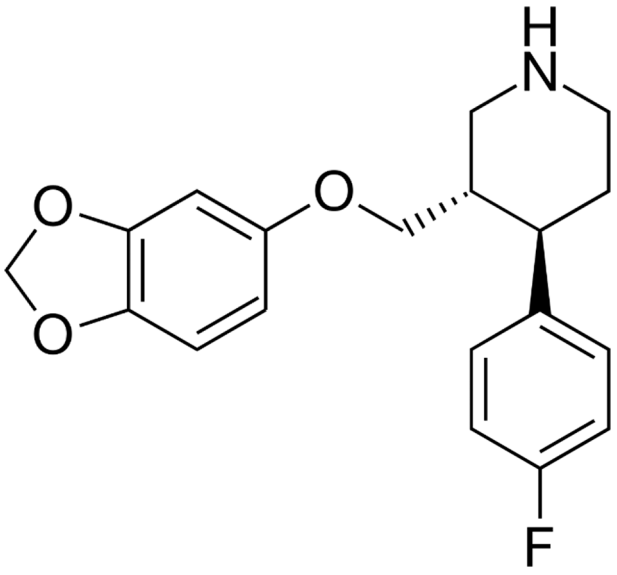

Fig. 1. Structure of PARO.

interaction mechanism. These signals can also provide data regarding interaction mode at the surface or in the solution.

Paroxetine, (PARO) a phenylpiperidine derivative (Fig. 1), is an effective serotonin reuptake inhibitor (SSRI) and is employed well for treating depressive and anxiety illnesses as depression, various OCSs (obsessive compulsive disorders), panic syndrome, and agoraphobia for a wide age range [1,12]. It is also recommended for treating the premenstrual dysphoric disorder, common anxiety disorders, post-traumatic stress disorder, presumed serotonergic component, and persistent headache.

Though PARO is a relatively weak norepinephrine (NE) uptake inhibitor, it still performs better at this site compared to the other SSRIs. The selectivity (ratio of inhibition of uptake of norepinephrine to serotonin NE/5-HT) of PARO is highest amongst other SSRIs [13,14]. PARO also does have a slight affinity towards catecholaminergic, dopaminergic, or histaminergic systems and, compared to tricyclic antidepressants (TCAs), has a low chance of causing central and autonomic side effects. Furthermore, the adaptive variations of somatodendritic (5-HT_{1A}) and terminal (5-$HT_{1B/1D}$) auto-receptors observed in the case of PARO are not the same as those of TCAs as it also plays a role to inhibit nitric oxide synthase. PARO can serve as a substrate as well as an inhibitor of cytochrome isoenzyme P450 2D6 [13]. It is orally absorbable and undertakes large first-pass metabolism that is partly saturable. Thus, PARO is proven to be a highly effective and well-tolerated drug that is an appropriate first-line treatment for depression. Besides its antidepressant properties, the anticancer effects of PARO for various cancer cells have been reported in some studies. Some researches about the use of PARO in cancer patients has showed that its use is associated with decreased risks of colorectal cancer and epithelial ovarian cancer, whereas its effect on breast cancer outcome is controversial [15–18].

To the best of our knowledge, there is no literature available so far on the interaction study of PARO and DNA through electroanalytical methods. To get an insight of its action mechanism, this study intends to explore the interaction between PARO and double-stranded calf thymus DNA (ct-dsDNA) by modifying glassy carbon electrode (GCE) surface with multilayer ct-dsDNA and in solution phase studies by differential pulse voltammetry (DPV). To confirm the interaction results as well as to calculate binding constants and thermodynamic parameters, fluorescence emission spectroscopy was performed. Furthermore, to get a detailed insight, the biosensor interaction of PARO with polyadenine (polyA) was carried out.

2. Materials and methods

2.1. Reagents and chemicals

PARO was supplied from Sanovel (Istanbul, Turkey). ct-dsDNA and polyA were purchased from Sigma Aldrich (USA). Stock solutions of the supporting electrolyte were made using analytical grade reagents and ultra-pure water from a Millipore Milli-Q system. The solutions prepared were stored at 4 °C. Spectroscopic and voltammetric measurements were performed using acetate buffer solution (0.1 M, pH4.7, ABS) as a supporting electrolyte.

2.2. Instrumentation and apparatus

Fluorescence spectrophotometer (Agilent Cary Eclipse Fluorescence Spectrophotometer) used in this study and quartz fluorescence cuvette of 10 mm × 10 mm dimensions to hold the sample. Scanning - fluorescence emission spectrum excitation wavelength (λ_{ex}) was set at 285 nm; emission wavelength range was set from 285 nm to 435 nm. The spectral bandpass was set at 10 nm.

AUTOLAB-PGSTAT 204 (Eco Chemie, Utrecht, Netherlands) running with NOVA 2.1 software was used to perform all voltammetric measurements. Scans were obtained using a classical three-electrode system; a glassy carbon electrode (GCE) (φ = 3.0 mm) was used as a working electrode, reference electrode consists of Ag/AgCl (BASi; 3 M NaCl), and an auxiliary electrode is a platinum wire. A SevenCompact™ pH/Ion S220 model (Mettler Toledo, Switzerland) with a combined glass reference electrode was used to adjust the pH of solutions.

2.3. Fluorescence analyses

The fluorescence data of varying concentrations of PARO and 0.3 μM ct-dsDNA mixtures were obtained by spectrofluorometer at 293 K, 298 K, 303 K, and 310 K regulated by a Peltier temperature controller. 285 nm as an excitation wavelength, 10 nm as an excitation, and emission slits, and 600 V as a photomultiplier tube voltage were selected to carry out these studies.

2.4. Electrochemical measurements

The electroanalytical studies were carried out by DPV using anodic scan mode, with a scan rate of 5 mV s^{-1}. The DPV voltammograms presented were of PARO prepared in ultra-pure water as 1 mM and diluted to the desired concentration by acetate buffer (0.1 M, pH 4.7). The buffer was made by combining predetermined amounts of 0.1 M sodium acetate and 0.1 M acetic acid solutions. Before commencement of each measurement, the surface of GCE was thoroughly polished with alumina slurry (particle size: 0.05 μm) on a polishing pad. Following each measurement, moving average application was used for baseline correction of all experimental voltammograms.

2.5. In-solution electrochemical studies

In-solution studies for the PARO-ct-dsDNA were carried out to evaluate the binding constant (with 500 μg/mL of ct-dsDNA and varying concentration of PARO) stirred for 3 min to reach binding equilibrium. Also, in-solution studies were carried out with 300 μg/mL DNA and 30 μM PARO peaks in ABS (pH 4.7) for varied interaction times from 1 min to 120 min. This experiment with the same conditions was repeated with 300 μg/mL polyA.

2.6. Biosensor fabrication

Thorough polishing of GCE was done on a polishing pad employing an alumina slurry of 0.05 μm diameter. Polished GCE was then rinsed with a jet of ultra-pure water and was dried in air. Multilayer ct-dsDNA

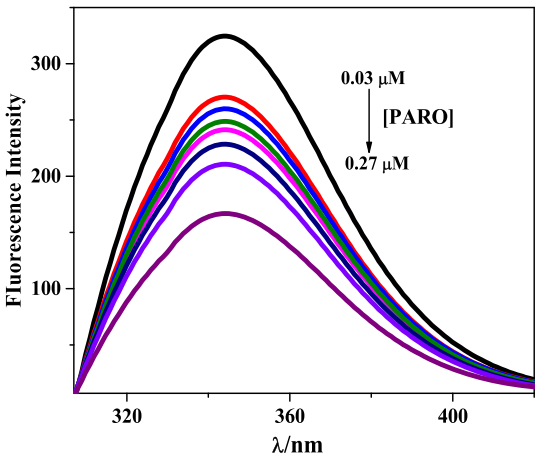

Fig. 2. Fluorescence spectra of different concentrations of PARO (0.03 μM, 0.038 μM, 0.05 μM, 0.058 μM, 0.087 μM, 0.142, 0.264 μM) bound to 0.5 μM ct-dsDNA at 30 °C.

Table 1
Thermodynamic parameters, the number of binding sites (n), and binding constant for the binding of PARO to ct-dsDNA.

Temperature (K)	n	K 10^4/mol^{-1}dm^3	-Δ*G* kJmol^{-1}	Δ*H*kJmol^{-1}	Δ*S*Jmol^{-1}K^{-1}
293	0.616	1.078	22.6	76.03	0.284
298	0.647	1.58	23.95		
303	0.676	2.52	25.53		
310	0.774	5.32	27.4		

biosensor was fabricated by casting 5 μL solution of 50 μM ct-dsDNA (prepared freshly) on the GCE surface thrice. After casting a drop on the surface of the electrode, the ct-dsDNA layer was held to stand at 40 °C temperature in a vacuum oven until it was dried completely. Afterward, the prepared DNA biosensor was cleaned by immersion into 0.1 M, pH 4.7, ABS for 1 s to remove the unbound ct-dsDNA from the surface of electrode. Finally, the biosensor was rinsed with ultra-pure water. The ct-dsDNA biosensor was immersed in an PARO solution, and was incubated for different time periods. Then, the biosensor was cleaned again with ABS for 5 s to remove any unbound PARO. DP voltammograms were recorded in a cleaned 0.1 M, pH 4.7, ABS in the potential range of 0.2 and 1.5 V. Each steps were performed with a new DNA biosensor.

2.7. Molecular docking studies

The molecular docking studies were carried out using Glide implemented in the Schrödinger Small-Molecule Drug Discovery Suite (Small-Molecule Drug Discovery Suite 2021–4, Schrödinger, LLC, New York, NY, 2021). PARO, which was built *via* builder panel in Maestro, was subjected to ligand preparation by LigPrep (Schrödinger Release 2021–4: LigPrep, Schrödinger, LLC, New York, NY, 2021) using default conditions. The X-ray crystal structures of DNA intercalators, PDB IDs 1XRW [19] and 1Z3F [20], were retrieved from the Protein Data Bank. The DNA fragments were prepared using the Protein Preparation Wizard tool. Water molecules were deleted, and hydrogen atoms were added, followed by the assignment of all-atom charges and atom types. Finally, energy minimization and refinement of the structures were done up to 0.3 Å RMSD by applying OPLS4 force field. Since the receptor grid generation tool is not parametrized for generating grid files with metal atoms, the only acridine part of the co-crystalized ligand was kept in DNA structure, PDB ID:1XRW. Further, the centroid of the co-crystalized ligands were defined as the grid box and van der Waals (vdW) radius

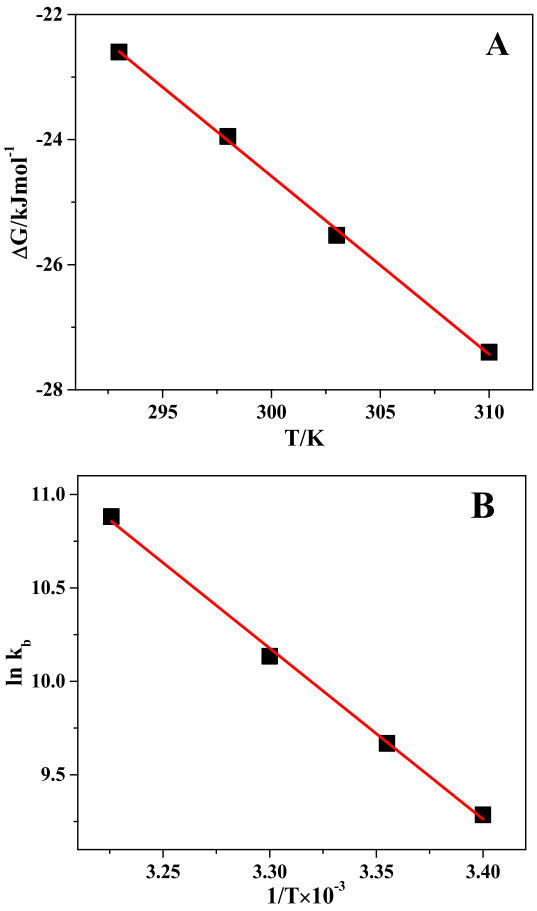

Fig. 3. A) Van't Hoff plot for the PARO - ct-dsDNA complex fluorescence results (y = −0.284x + 60.87; R^2 = 0.990), B) Plots of ln K versus 1/T at different temperatures (y = −9145.51x + 40.36; R^2 = 0.990).

scaling factor 1.00, partial charge cutoff 0.25, and OPLS4 force field were used for receptor grid generation. The docking protocol was justified by redocking of co-crystallized ligand. PARO was docked into ct-dsDNA structures using the standart precision (SP) docking mode of the Glide without any constraints and a 0.80 vdW radius scaling factor and 0.15 partial charge cutoff [21].

3. Results and discussion

3.1. Steady-state fluorescence and the mode of fluorescence quenching

Fluorescence spectra is an excellent tool for qualitative analysis of PARO to the ct-dsDNA binding. Fluorescence quenching provides direct evidence of molecular interactions as diminishing fluorescence intensity of a fluorophore can be observed upon molecular interactions [22,23]. These molecular interactions could be due to relocations of molecular structures, activated-state reactions, energy transmission processes, collisional quenching, or ground-state complex formation. Quenching may be dynamic or static quenching. In both quenching types, the basic requirement is the molecular contact between the quencher and the fluorophore [8,11]. Fluorophore and quencher encounter each other during the excited state lifetime for dynamic quenching. Fluorophore returns to the ground state with no emission upon contact with the quencher [7]. On the contrary, in static quenching mode, a nonfluorescent complex is formed by the fluorophore and quencher. Static and dynamic quenching depends differently on temperature and viscosity. Dynamic quenching rises at elevated temperatures due to a faster rate of diffusion. While static quenching decreases at higher temperatures as the weakly bound complexes dissociate at higher

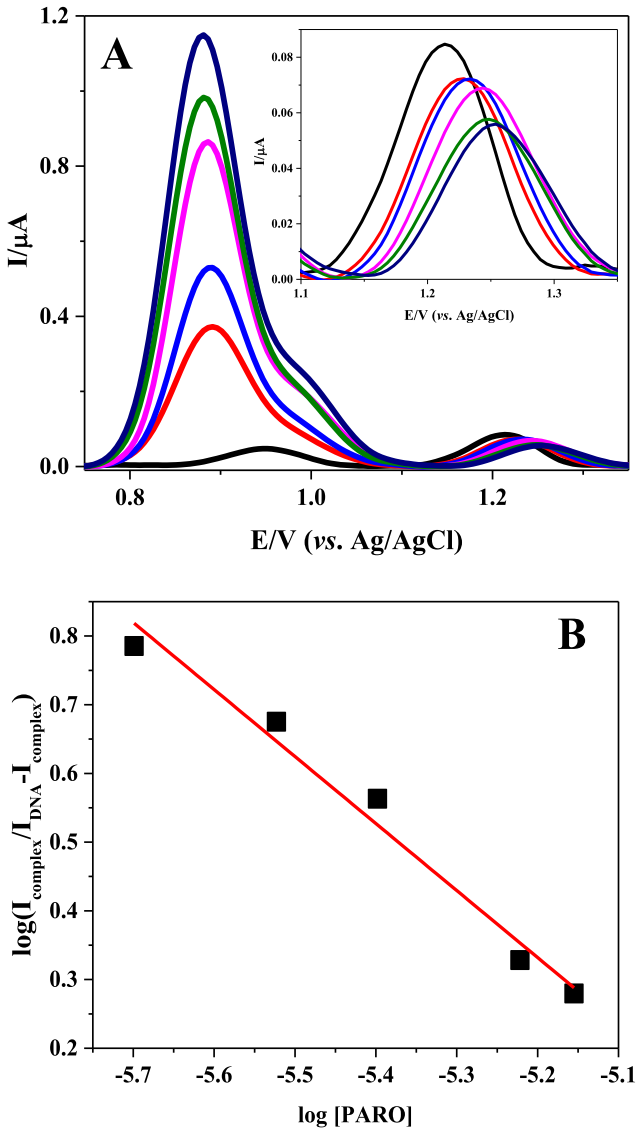

Fig. 4. A) DP voltammograms of 500 ppm ct-dsDNA with successive addition of various concentrations of PARO (2 μM, 3 μM, 4 μM, 6 μM, 7 μM) and interaction studies on GCE, B) Relation of $\log\left(\frac{I_{complex}}{I_{DNA}-I_{complex}}\right)$ *vs* log concentration of PARO in the range of 2 μM to 7 μM (y = -0.975x + 4.74; R^2 = 0.990).

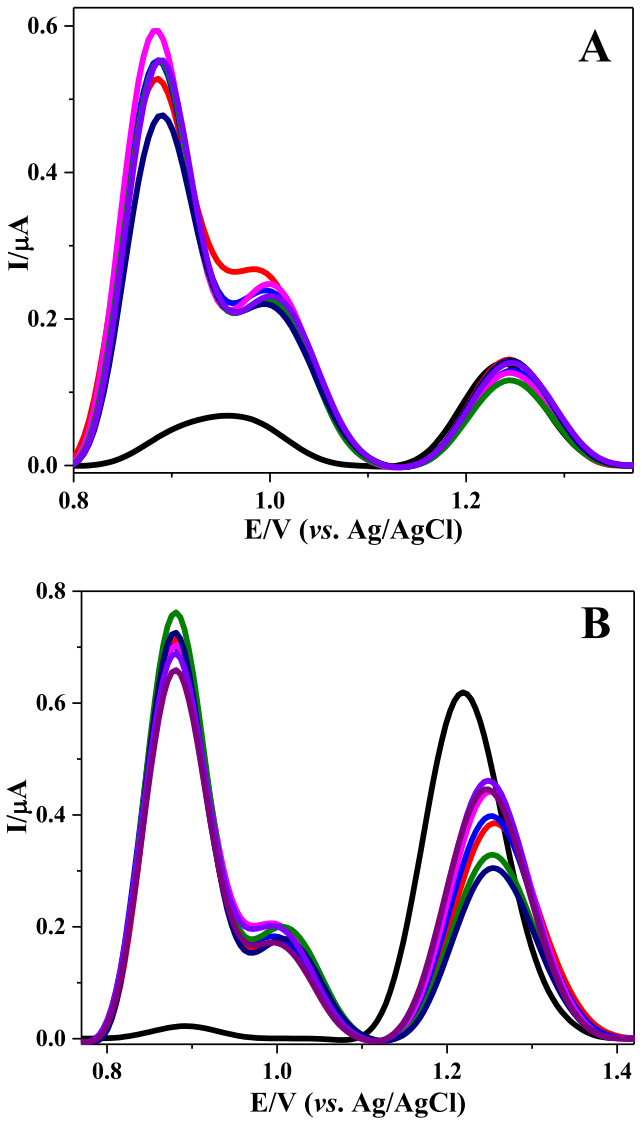

Fig. 5. A) DPV responses of 300 μg/mL ct-dsDNA and 30 μM PARO peaks in ABS 4.7 for interaction times, 1–120 min on GCE (black DNA, red 1 min, blue 5 min, pink 30 min, green 60 min, dark blue 90 min, purple 120 min), B) DPV responses of adenine peaks after interaction with 30 μM PARO in ABS 4.7 for 1–120 min on GCE. (black polyA, pink 1 min, red 5 min, green 30 min, dark blue 60 min, purple 90 min, dark purple 120 min).

Table 2
DNA binding constants of some antidepressant drugs at room temperature.

Drug	DNA binding constant (M^{-1})	Proposed binding mode	Reference
Amsacrine	–	Intercalative mode	[31]
Aripiprazole	3×10^5	Hydrophobic and hydrophilic interactions	[32]
Buzepide	1.908×10^5	Intercalation	[4]
Citalopram	5.01×10^3	Electrostatic interactions	[33]
Escitalopram	3.31×10^4	Groove binding	[33]
Fluoxetine	6.7×10^4	Groove binding	[34]
Imipramine	–	Intercalation	[5]
Sertraline	8.34×10^3	Groove binding	[35]
Paroxetine	7.24×10^4	Intercalation mode	This work

temperatures [7–9]. In some instances, quenching of the fluorophore by collisions and complex formation take place simultaneously. In that situation, nature changes and show an upward curvature.

When excitation wavelength was set as 285 nm, PARO exhibited a maximum emission peak at 340 nm. The fluorescent emission spectra of PARO as with ct-dsDNA can be seen in Fig. 2. It can be seen from Fig. 2 that there is a significant diminution in the intrinsic fluorescence of PARO when its fixed concentration is titrated against ct-dsDNA. The quenching observed can be attributed to the fact that photoelectrons are transmitted from the bases to the intercalator's excited state when an interaction with the intercalator and the base pairs of ct-dsDNA takes place results in the quenching of the fluorescence intensity. As the PARO emission intensity at 340 nm decreased considerably, it advocates the intercalation mode of interaction between PARO and ct-dsDNA, and this type of interaction process follows the Stern-Volmer equation (1) [24].

$$\frac{F_o}{F} = 1 + K_q \tau_o [D] = 1 + K_{sv}[D] \quad (1)$$

Here, F_0 is the fluorescence intensity of PARO before quenching, and F is the fluorescence intensity of complex after successive additions of ct-dsDNA, K_q represents the rate constant of bimolecular collision, the average life span of fluorescent molecules τ_0 is about 10 ns, [D] refers to

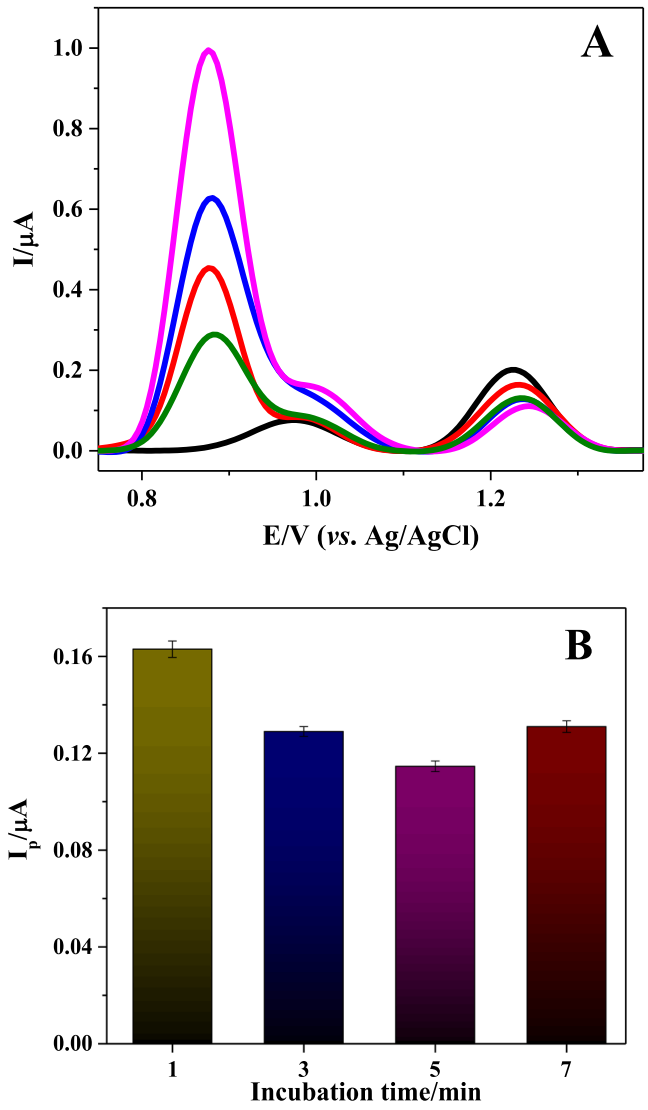

Fig. 6. A) DPV responses of guanine and adenine peaks after interaction with 30 μM PARO for 1–7 min on ct-dsDNA/GCE (black DNA, red 1 min, blue 3 min, pink 5 min, green 7 min, dark), B) Bar chart related to interaction time studies.

the equilibrium concentration of ct-dsDNA (μM), K_{sv} is the Stern-Volmer quenching constant. Linear fitting [D] with F_0/F gives the quenching constants K_q and K_{sv} of the PARO - ct-dsDNA system from the slope.

3.2. Evaluation of binding constant and number of binding sites

The Lineweaver-Burk double logarithmic equation (2) can be applied on PARO-dsDNA system to evaluate binding constants K_b and the number of binding sites n [25,26].

$$\log\left(\frac{F_o - F}{F}\right) = logK_A + nlog[D] \quad (2)$$

K_a and n values obtained at different temperatures are tabulated in Table 1. It can be seen from Table 1 that temperature is driving the binding ability of the complex formed. Where the n representing the number of base pairs per bound ligand and it is an important parameter indicating the sites available for drug-DNA interaction. In the present case its value ranges from 0.616 to 0.774 at temperatures studied and increases with increase in temmperature. It suggests that higher temperature favours the binding as is also indicated by value of binding constant. The value of K_b obtained from fluorescence studies is in the

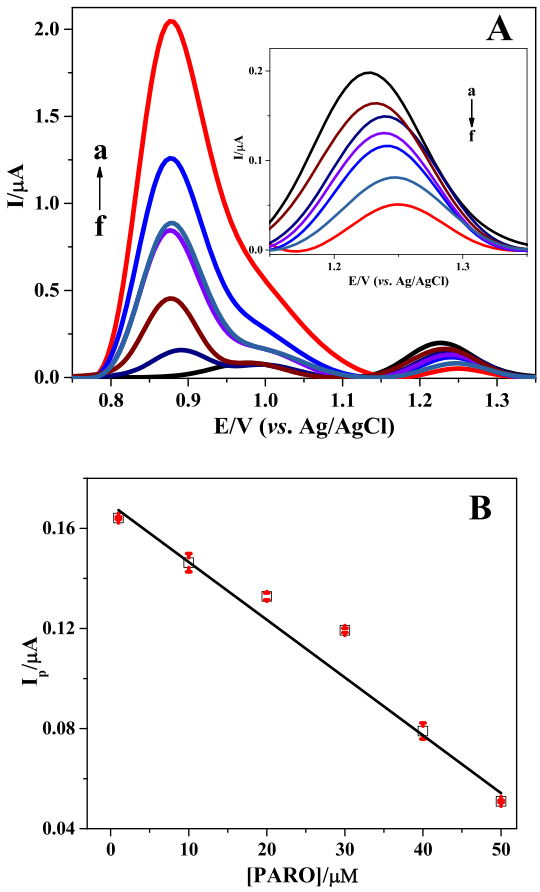

Fig. 7. A) DPV responses of adenine peaks after interaction with 1–50 μM PARO for 5 min on ct-dsDNA/GCE, B) Relation of current *vs* concentration of PARO.

Table 3
Regression data for determination of PARO by following the adenine signals at ct-dsDNA/GCE.

Parameters	Adenine
Measured potential (mV)	1250
Linearity range (μM)	1–50
Slope (A M^{-1})	0.0023
Correlation coefficient (*r*)	0.97
SE of slope	2.56×10^{-4}
LOD (μM)	0.29
LOQ (μM)	0.97
Repeatability of peak current (RSD%) *	1.59

orders of magnitude 10^4 as obtained from the electrochemical method. The little discrepancy arises due to differences in the overlying principle of both techniques.

3.3. Thermodynamics of PARO and ct-dsDNA binding event by fluorescence spectroscopy

The thermodynamics of drug-DNA binding offers valuable insight into the whole event. It also provides a significant understanding of the molecular forces participating in the complex formation and aid in estimating the free energies of ligand binding [7]. Comprehensive thermodynamic profiles offer a standpoint for analyzing thermodynamical parameters and their correlation with the structural features. It also provides an insight into DNA conformational changes upon accommodation of intercalators and restriction in the translational and rotational movements when the complex is formed. Both cases implicate

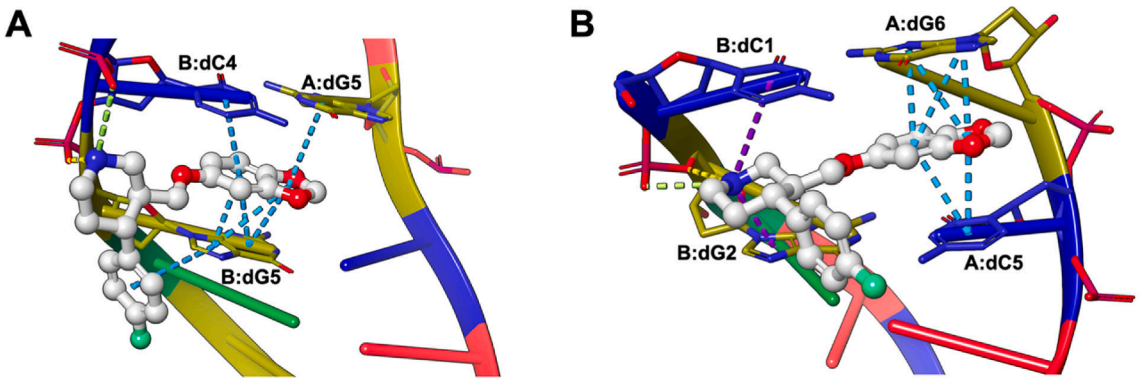

Fig. 8. Representative DNA binding modes of paroxetine (white ball and stick) obtained from molecular docking studies A) PDB ID: 1XRW with a binding score of −6.613 kcal/mol, B) PDB ID: 1Z3F with a binding score of −6.590 kcal/mol. The panels depict the π-π interactions (dashed cyan lines), salt bridges (dashed cyan lines), hydrogen bonds (dashed yellow lines), and π-cation interactions (dashed purple lines) between PARO and DNA base pairs.

unfavorable free energy for binding. This unfavorable free energy barrier is compensated by the various processes that offer additional free energy contributions to the overall process, including the transfer of ligand from solution to the binding site (hydrophobic), molecular interactions, and the polyelectrolyte contributions by ion release.

Thermodynamic parameters for interaction were calculated by using the following equation (3) for the gibbs free energy, equation (4) for the enthalpy change (ΔH) and equation (5) for the entropy change (ΔS).

$$\Delta G = -RTlnK \tag{3}$$

$$lnK = -\frac{\Delta H}{RT} \tag{4}$$

$$\Delta G = \Delta H - T\Delta S \tag{5}$$

Complex formation between PARO and ct-dsDNA was studied at different temperatures to determine various thermodynamic parameters in Fig. 3. In the case of minor groove binding, interacting species interact primarily through hydrophobic interactions. In contrast, in the case of intercalation mode, the small molecules intercalate into a ct-dsDNA duplex, which is stabilized by hydrophobic interactions and van der Waals forces. It is a well-established fact that in the case when $\Delta H < 0$ or $\Delta H = 0$ and $\Delta S > 0$, an electrostatic force is the central driving non-covalent force, while if $\Delta H > 0$ and $\Delta S > 0$, hydrophobic interactions are deemed as the main driving force as observed in the present case. Hydrogen bonds and van der Waals interaction show a thermodynamic profile where $\Delta H < 0$ and $\Delta S < 0$. The thermodynamic profile of the complex formed between PARO and ct-dsDNA supports the intercalation mode of interaction.

3.4. Electrochemical experiments in PARO and ct-dsDNA interaction

Interactions between DNA and small molecule forms the complex, which subsequently varies the amount of free DNA and target molecules in the solution, thus altering the oxidation signals of ct-dsDNA. Hence, electrochemical techniques are more often used for monitoring DNA-drug interactions. Electrochemistry is a valuable analytical tool to provide an insight into DNA-drug binding and helps to elucidate interaction mechanisms. Intercalative interaction mode is often associated with oxidation peak potential shifting towards more positive potential, while in the case of electrostatic interaction, oxidation potential shifts to a more negative value. Thus, in the present case, a positive shift in peak potential observed indicates that PARO interacts with ct-dsDNA through an intercalative mode of interaction. Firstly, before the successive concentrations of PARO were added into the ct-dsDNA solution, relative standard deviation (RSD%) values of deoxyguanosine (dGuo) and deoxyadenosine (dAdo) peak currents and peak potentials were evaluated with 5 different measurements using a bare GCE. RSD% values were obtained between 2.3 % and 3.2 %. FDA Guidance suggested that precision must lie within 15 % RSD for a reproducible biosensor [27,28]. Therefore, the obtained results showed that the PARO-ct-dsDNA interaction can be evaluated in the insolution phase. Moreover, as the biosensor designed to evaluate the interaction of ct-dsDNA with PARO is disposable so its repeatability was confirmed. For this purpose, prior to interaction studies, 5 different ct-dsDNA biosensors were prepared on the same day and their repeatability was checked. Repeatability was also evaluated on the different days. The intraday, and interday RSD% values were calculated considering the current values of dGuo and dAdo, and RSD% values were found between 2.1 % and 2.9 %. Thus, the calculated results confirmed that the prepared ct-dsDNA biosensor for evaluating PARO interaction is reproducible.

DPV technique compared to CV offers greater sensitivity and superior peak resolution for analyzing the electrochemical behavior of biological systems, so DPV was used to study PARO- ct-dsDNA interaction in the following experiments [3,29]. Prior to each successive scan, the PARO- ct-dsDNA solution mixture was stirred for 3 min to reach binding equilibrium. GCE worked as a transducer in this study to probe the interactions between ct-dsDNA and PARO electrochemically. Successive concentrations of PARO were put in onto the ct-dsDNA solution, and the obtained oxidation peak signals were recorded as DP voltammograms. For only the ct-dsDNA solution, two distinct peaks corresponding to the oxidation of dGuo at potential + 0.94 V and dAdo at potential 1.21 V were obtained.

As the oxidation peaks of PARO overlapped with the dGuo peak, affecting dGuo peak current as well as peak potential thus, only the variations in the dAdo peak were monitored to decipher the interaction. As shown in Fig. 4, the dAdo peak height decreased with successive addition of PARO solution, suggesting the PARO- ct-dsDNA complexation in the solution. Moreover, the peak potential moved towards a further positive value with the subsequent addition of drug concentration. Bard et al. illustrated that electrostatic interactions often lead to negative shifts while the positive shifts in peak potential of intercalators are attributed to binding via a hydrophobic mode of interactions (intercalation) [30]. Thus, it is suggested that the shift of peak potential observed in the case of PARO can be due to the planar aromatic ring structure of PARO that facilitates its intercalation into the DNA helix.

Based on the drop in the dAdo peak current upon binding, the binding constants (K) of PARO was determined by using the following equation (6):

$$\log\left(\frac{I_{complex}}{I_{DNA} - I_{complex}}\right) = nlogK - nlogC_{drug} \tag{6}$$

where I_{DNA} is the peak current of dAdo in the absence of PARO and $I_{complex}$ is the peak current presence of different concentrations of PARO. By linear regression of $\log\left(\frac{I_{complex}}{I_{DNA}-I_{complex}}\right)$ on $logC_{drug}$], stoichiometry of the

complexes and binding constant values can be calculated. Value of n obtained from slope of equation is 0.975. The slope value shows that only one PARO complex binds to each ds-ctDNA. Based on the intercept of the plot of $\log\left(\frac{I_{complex}}{I_{DNA}-I_{complex}}\right)$ vs $logC_{drug}$, K was determined as 7.24×10^4 M^{-1} (Fig. 4).

Table 2 demonstrates the mode of interaction and corresponding binding constant values for various antidepressant drugs studied in the previous years. Antidepressants like citalopram and sertraline bind mildly via electrostatic or groove binding mode with ds-ctDNA with binding constant values equal to 10^3 or lesser. PARO follows the profile of structurally comparable buzepide and binds with ds-ctDNA through a strong intercalative mode.

Electrochemical interaction for PARO -ct-dsDNA and PARO-polyA was also explored in 0 min, 5 min, 30 min, 60 min, and 120 min incubation times by DPV. For this, and concentration of ct-dsDNA taken was 300 μg/mL while that of PARO was 30 μM. 300 μg/mL polyA and 30 μM PARO was also scanned under the same conditions in the identical incubation times. No significant changes were observed after 60 min for both systems. The interaction with PARO leads to a decrease in adenine signals till 60 min, after which it becomes constant. PolyG signals were not tracked as the drug and polyG do have nearly identical potentials, so there are fair chances of overlapping the signals and hence biased results (Fig. 5).

3.5. Effect of incubation time of PARO on analytical signals

Interaction time was optimized to attain the highest optimum PARO loading on the ct-dsDNA/GCE surface. The binding of PARO to ct-dsDNA was found dependent on immersion of ct-dsDNA/GCE in PARO solution for different interaction times. In solution studies showed that the oxidation peaks of PARO overlapped with the dGuo peak, affecting dGuo peak current as well as peak potential; thus, only the variations in the dAdo peak were monitored to decipher the interaction [36]. The same was observed in the case of the biosensor. Therefore, the change in dAdo peak height was monitored to find the analytical parameters. When the interaction time was increased from 1 to 5 min, a decrease in dAdo peak was observed, which became constant; then thus 5 min incubation time was chosen as optimum interaction time for the subsequent experiments (Fig. 6).

3.6. PARO concentration effect on dAdo analytical signal

DP voltammograms at different concentrations of PARO (1–50 μM) on ct-dsDNA/GCE. The DPV results were obtained in an ABS of pH4.7, and for each concentration of PARO, ct-dsDNA/GCE was incubated for 5 min in the respective drug solution. The oxidation signals of adenine were found to be decreasing with increasing concentrations of PARO. The peak currents of adenine showed a linear trend with PARO concentration over the range of 1–50 μM with *"r"* values of 0.99 (Fig. 7).

To validate the sensitivity of the electrode developed, the limit of detection (LOD) and limit of quantification (LOQ) values were evaluated by the following equations (7) and (8).

$$LOD = 3\frac{s}{m} \tag{7}$$

$$LOQ = 10\frac{s}{m} \tag{8}$$

Here '*s*' denotes the standard deviation while '*m*' is the slope of the calibration curve [37,38]. Using calibration curves, the LOD value for PARO obtained from adenine base signals was estimated as 0.29 μM. Obtained analytical parameters obtained using calibration curve were tabulated in Table 3.

3.7. DNA binding mode analysis of PARO

It is reported that the accuracy of DNA docking protocol is directly associated with choosing the suitable DNA template, and according to the experimental indication concerning the nature of the interaction of a molecule with DNA is known, that is, intercalator, a DNA structure with intercalation gaps should be selected [39]. Given the fact that there are two types of intercalator molecules, including classic intercalators and threading intercalators [28,40], two types of DNA structure containing intercalation gaps *(i)* dsDNA-classic intercalator complex with two intercalation gaps (PDB ID: 1Z3F), and *(ii)* dsDNA-threading intercalator complex with only one intercalation gap (PDB ID: 1XRW) were used for molecular docking simulations in order to elucidate the binding mode of PARO, which was shown to intercalate with DNA as a result of spectroscopic (and electrochemical) studies. The docked results presented in Fig. 8 showed that PARO exhibited a similar interaction pattern, and the insertion of PARO occurred into the CG intercalation site, as with the most intercalators [41].

PARO was found to be inserted between two flanking GC base pairs and formed π-π interactions by its benzodioxole ring, the planar section, which was the main driving force of the intercalation binding mode. The other part with the fluorophenyl substituted piperidine ring exposed in the minor groove between B:dC4 and B:dG5 (for PDB ID: 1XRW); B: dC1and B:dG2 (for PDB ID: 1Z3F) forming hydrogen bonds, π-cation interactions, and salt bridges obtained *via* the positively charged nitrogen atom of piperidine ring, and a π-π interaction through phenyl ring, which contribute to the formation of DNA-PARO intercalation complex.

4. Conclusion

In this study, the electrochemical interaction of ct-dsDNA and PARO, a phenylpiperidine-based drug, was examined for the first time. Voltammetric and spectrophotometric methods were used to investigate the interaction between PARO and ct-dsDNA, and docking studies were conducted to confirm the experimental results. The findings indicated that the interaction between PARO and ct-dsDNA occurred via the intercalation mode with a binding constant value of 7.24×10^4 M^{-1} and 1.52×10^4 M^{-1} at 25 °C, based on voltammetric and spectroscopic results, respectively. The negative values of the change in the Gibbs free energy suggested that the PARO– ct-dsDNA complex formation is a spontaneous process. Oxidation of drug was employed as a sensitive procedure for the PARO- ct-dsDNA interaction determination in the concentration range of 1 to 50 μM with a LOD value of 0.29 μM. The short analysis time, cost-effectiveness, and simplicity were the main pros of the presented voltammetric procedure. Furthermore, the developed method demonstrated improved analytical properties regarding low LOD values.

CRediT authorship contribution statement

Rafia Nimal: Software, Validation, Formal analysis, Writing – original draft. **Didem Nur Unal:** Methodology, Validation, Writing – review & editing. **Cem Erkmen:** Methodology, Validation, Writing – review & editing. **Sevinc Kurbanoglu:** Methodology, Validation, Writing – review & editing. **Muhammad Siddiq:** Writing – review & editing. **Gokcen Eren:** Writing – review & editing. **Afzal Shah:** Writing – review & editing. **Bengi Uslu:** Conceptualization, Methodology, Writing – review & editing, Supervision.

Declaration of Competing Interest

The authors declare that they have no known competing financial interests or personal relationships that could have appeared to influence the work reported in this paper.

Data availability

Data will be made available on request.

Acknowledgement

Rafia Nimal is grateful to Turkiye Burslari research scholarship for funding her visit to Ankara, Turkey. The Council of Higher Education (YOK) was greatly appreciated for providing scholarships under the special 100/2000 scholarship program to Cem Erkmen and Didem Nur Unal. Cem Erkmen also acknowledges the financial assistance provided by the The Scientific and Technological Research Council of Türkiye (TUBITAK) under the BIDEB/2211-A doctoral scholarship program.

References

[1] R.J. Milne, K.L. Goa, Citalopram: A Review of its Pharmacodynamic and Pharmacokinetic Properties, and Therapeutic Potential in Depressive Illness, Drugs. 41 (1991) 450–477, https://doi.org/10.2165/00003495-199141030-00008.
[2] G.A. Tiğ, B. Zeybek, Ş. PekyardImcı, Electrochemical DNA biosensor based on poly (2,6-pyridinedicarboxylic acid) modified glassy carbon electrode for the determination of anticancer drug gemcitabine, Talanta. 154 (2016) 312–321, https://doi.org/10.1016/j.talanta.2016.03.049.
[3] L. Qian, S. Durairaj, S. Prins, A. Chen, Nanomaterial-based electrochemical sensors and biosensors for the detection of pharmaceutical compounds, Biosens. Bioelectron. 175 (2021), 112836, https://doi.org/10.1016/j.bios.2020.112836.
[4] S. Kurbanoglu, B. Dogan-Topal, L. Hlavata, J. Labuda, S.A. Ozkan, B. Uslu, Electrochemical investigation of an interaction of the antidepressant drug aripiprazole with original and damaged calf thymus dsDNA, Electrochim. Acta. 169 (2015) 233–240, https://doi.org/10.1016/j.electacta.2015.04.087.
[5] J. Jankowska- Śliwińska, M. Dawgul, D.G. Pijanowska, DNA-based electrochemical biosensor for imipramine detection, Procedia Eng. 120 (2015) 574–577, https://doi.org/10.1016/j.proeng.2015.08.727.
[6] B. Rafique, A.M. Khalid, K. Akhtar, A. Jabbar, Interaction of anticancer drug methotrexate with DNA analyzed by electrochemical and spectroscopic methods, Biosens. Bioelectron. 44 (2013) 21–26, https://doi.org/10.1016/j.bios.2012.12.028.
[7] D.P. Remeta, K.J. Breslauer, C.P. Mudd, R.L. Berger, Thermodynamic Characterization of Daunomycin-DNA Interactions: Comparison of Complete Binding Profiles for a Series of DNA Host Duplexes, Biochemistry. 32 (1993) 5064–5073, https://doi.org/10.1021/bi00070a014.
[8] C. Pérez-Arnaiz, N. Busto, J.M. Leal, B. García, New insights into the mechanism of the DNA/doxorubicin interaction, J. Phys. Chem. B. 118 (2014) 1288–1295, https://doi.org/10.1021/jp411429g.
[9] F. Leng, J.B. Chaires, M.J. Waring, Energetics of echinomycin binding to DNA, Nucleic Acids Res. 31 (2003) 6191–6197, https://doi.org/10.1093/nar/gkg826.
[10] M. Chien, A.P. Grollman, S.B. Horwitz, Bleomycin-DNA Interactions: Fluorescence and Proton MagneticResonance Studies, Biochemistry. 16 (1977) 3641–3647.
[11] G.T.H. Nguyen, W.Y. Leung, T.N. Tran, H. Wang, V. Murray, W.A. Donald, Mechanism for the Binding of Netropsin to Hairpin DNA Revealed Using Nanoscale Ion Emitters in Native Mass Spectrometry, Anal. Chem. 92 (2020) 1130–1137, https://doi.org/10.1021/acs.analchem.9b04209.
[12] S.W. Tang, D. Helmeste, Paroxetine, Expert Opin. Pharmacother. 9 (2008) 787–794, https://doi.org/10.1517/14656566.9.5.787.
[13] M. Bourin, P. Chue, Y. Guillon, Paroxetine: A Review, CNS Drug Rev.7 (2001) 25–47. https://doi.org/ 10.1111/j.1527-3458.2001.tb00189.x.
[14] D.L. Musselman, D.H. Lawson, J.F. Gumnick, A.K. Manatunga, S. Penna, R.S. Goodkin, K. Greiner, C.B. Nemeroff, A.H. Miller, Paroxetine for the Prevention of Depression Inducedby High-Dose Interferon Alfa, N. Engl. J. Med. 344 (2001) 961–966 https://doi.org/ 10.1056/NEJM200103293441303.
[15] W. Xu, H. Tamim, S. Shapiro, M.R. Stang, J.P. Collet, Use of antidepressants and risk of colorectal cancer: A nested case-control study, Lancet Oncol. 7 (2006) 301–308, https://doi.org/10.1016/S1470-2045(06)70622-2.
[16] L.S. Mørch, C. Dehlendorff, L. Baandrup, S. Friis, S.K. Kjær, Use of antidepressants and risk of epithelial ovarian cancer, Int. J. Cancer. 141 (2017) 2197–2203, https://doi.org/10.1002/ijc.30919.
[17] J. Chubak, E.J.A. Bowles, O. Yu, D.S.M. Buist, M. Fujii, D.M. Boudreau, Breast cancer recurrence in relation to antidepressant use, Cancer Causes Control. 27 (2016) 125–136, https://doi.org/10.1007/s10552-015-0689-y.
[18] B. Liu, T. Yuan, C. Huang, D. Hsu, S. Chen, N. Hsiao, S. Lin, S. Wu, Y. J. Lin, S. Chuang, DNA repair proteins as the targets for paroxetine to induce cytotoxicity in gastric cancer cell AGS, 12 (2022) 1465–1483.
[19] H. Baruah, M.W. Wright, U. Bierbach, Solution structural study of a DNA duplex containing the guanine-N7 adduct formed by a cytotoxic platinum - Acridine hybrid agent, Biochemistry. 44 (2005) 6059–6070, https://doi.org/10.1021/bi050021b.
[20] A. Canals, M. Purciolas, J. Aymamí, M. Coll, The anticancer agent ellipticine unwinds DNA by intercalative binding in an orientation parallel to base pairs, Acta Crystallogr. Sect. D Biol. Crystallogr. 61 (2005) 1009–1012, https://doi.org/10.1107/S0907444905015404.
[21] T.A. Halgren, R.B. Murphy, R.A. Friesner, H.S. Beard, L.L. Frye, W.T. Pollard, J.L. Banks, Glide: A New Approach for Rapid, Accurate Docking and Scoring. 2. Enrichment Factors in Database Screening, J. Med. Chem. 47 (2004) 1750–1759. https://doi.org/10.1021/jm030644s.
[22] B.Y. Michel, D. Dziuba, R. Benhida, A.P. Demchenko, A. Burger, Probing of Nucleic Acid Structures, Dynamics, and Interactions With Environment-Sensitive Fluorescent Labels, Front. Chem. 8 (2020) 112, https://doi.org/10.3389/fchem.2020.00112.
[23] D. Musumeci, C. Platella, C. Riccardi, F. Moccia, D. Montesarchio, Fluorescence sensing using DNA Aptamers in cancer research and clinical diagnostics, Cancers (Basel). 9 (2017) 1–43, https://doi.org/10.3390/cancers9120174.
[24] W. Zhong, J.S. Yu, W. Huang, K. Ni, Y. Liang, Spectroscopic studies of interaction of chlorobenzylidine with DNA, Biopolym. - Biospectroscopy Sect. 62 (2001) 315–323, https://doi.org/10.1002/bip.10001.
[25] A. Sajid-ur-Rehman, G. Saeed, P.A. Saddique, F.A. Channar, Q. Larik, M. Abbas, H. Hassan, T.A. Raza, S.Y.S. Fattah, Synthesis of sulfadiazinyl acyl/aryl thiourea derivatives as calf intestinal alkaline phosphatase inhibitors, pharmacokinetic properties, lead optimization, Lineweaver-Burk plot evaluation and binding analysis, Bioorganic, Med. Chem. 26 (2018) 3707–3715, https://doi.org/10.1016/j.bmc.2018.06.002.
[26] B.K. Hamilton, C.R. Gardner, C.K. Colton, Effect of diffusional limitations on lineweaver-burk plots for immobilized enzymes, AIChE J. 20 (1974) 503–510, https://doi.org/10.1002/aic.690200310.
[27] R. Nimal, O. Selcuk, S. Kurbanoglu, A. Shah, M. Siddiq, B. Uslu, Trends in electrochemical nanosensors for the analysis of antioxidants, TrAC - Trends Anal. Chem. 153 (2022), 116626, https://doi.org/10.1016/j.trac.2022.116626.
[28] S. Kurbanoglu, B. Dogan-Topal, E.P. Rodriguez, B. Bozal-Palabiyik, S.A. Ozkan, B. Uslu, Advances in electrochemical DNA biosensors and their interaction mechanism with pharmaceuticals, J. Electroanal. Chem. 775 (2016) 8–26, https://doi.org/10.1016/j.jelechem.2016.05.022.
[29] A.G. dos Santos Neto, C.S. de Sousa, A. da Silva Freires, S.M. Silva, H. Zanin, F.S. Damos, R. de Cássia Silva Luz, Electrochemical sensor for detection of imipramine antidepressant at low potential based on oxidized carbon nanotubes, ferrocenecarboxylic acid, and cyclodextrin: application in psychotropic drugs and urine samples, J. Solid State Electrochem. 22 (2018) 1385–1394. https://doi.org/10.1007/s10008-017-3772-3.
[30] E. de S. Gil, G.R. de Melo, Electrochemical biosensors in pharmaceutical analysis, Brazilian J. Pharm. Sci. 46 (2010) 375–391. https://doi.org/10.1590/S1984-82502010000300002.
[31] H.M. Moghaddam, H. Beitollahi, G. Dehghannoudeh, H. Forootanfar, Electrochemical determination of amsacrine at a ds-DNA modified graphene carbon paste electrode and its application as a label-free electrochemical biosensor, Int. J. Electrochem. Sci. 12 (2017) 9958–9971, https://doi.org/10.20964/2017.11.39.
[32] S.S. Kalanur, J. Seetharamappa, S.N. Prashanth, Interaction of an antidepressant buzepide methiodide with DNA immobilized on the glassy carbon electrode, Colloids Surfaces B Biointerfaces. 82 (2011) 438–442, https://doi.org/10.1016/j.colsurfb.2010.09.017.
[33] Ç.K. Dindar, C. Erkmen, S. Yıldırım, B. Bozal-Palabiyik, B. Uslu, Interaction of citalopram and escitalopram with calf Thymus DNA: A spectrofluorometric, voltammetric, and liquid chromatographic approach, J. Pharm. Biomed. Anal. 195 (2021), 113891, https://doi.org/10.1016/j.jpba.2021.113891.
[34] S. Kashanian, S. Javanmardi, A. Chitsazan, K. Omidfar, M. Paknejad, DNA-binding studies of fluoxetine antidepressant, DNA Cell Biol. 31 (2012) 1349–1355, https://doi.org/10.1089/dna.2012.1657.
[35] P.S. Dorraji, F. Jalali, Investigation of the interaction of sertraline with calf thymus DNA by spectroscopic methods, J. Braz. Chem. Soc. 24 (2013) 939–945, https://doi.org/10.5935/0103-5053.20130123.
[36] A. Munir, B. Bozal-Palabiyik, G. Eren, A. Shah, S. Ali, N. Uddin, B. Uslu, Electrochemical Biosensor Design with Multi-walled Carbon Nanotube to Display DNA-Schiff Base Interaction, Electroanalysis. 33 (2021) 1761–1770, https://doi.org/10.1002/elan.202100156.
[37] S. Kurbanoglu, B. Uslu, S.A. Ozkan, Validation of Analytical Methods for the Assessment of Hazards in Food, Elsevier Inc., 2018. https://doi.org/10.1016/b978-0-12-814956-0.00004-4.
[38] O. González, R.M. Alonso, Validation of bioanalytical chromatographic methods for the quantification of drugs in biological fluids, in: Handb. Anal. Sep., Elsevier B. V., 2020: pp. 115–134. https://doi.org/10.1016/B978-0-444-64066-6.00006-X.
[39] M. Al-Rashida, S. Ahsen, In search of a docking protocol to distinguish between DNA intercalators and groove binders: Genetic algorithm vs. shape-complementarity based docking methods, RSC Adv. 5 (2015) 72394–72404, https://doi.org/10.1039/c5ra09929c.
[40] A. Soni, P. Khurana, T. Singh, B. Jayaram, A DNA intercalation methodology for an efficient prediction of ligand binding pose and energetics, Bioinformatics. 33 (2017) 1488–1496, https://doi.org/10.1093/bioinformatics/btx006.
[41] Y. Gilad, H. Senderowitz, Docking studies on DNA intercalators, J. Chem. Inf. Model. 54 (2014) 96–107, https://doi.org/10.1021/ci400352t.